Robotica: (2021) volume 39, pp. 1692–1710. © The Author(s), 2021. Published by Cambridge University Press.
doi:10.1017/S0263574720001447

Dynamic Modeling and Control of a Novel One-Legged Hopping Robot

Amin Khakpour Komarsofla, Ehsan Azadi Yazdi* and Mohammad Eghtesad

School of Mechanical Engineering, Shiraz University, Shiraz, Iran
E-mails: amin.khakpour93@yahoo.com, eghtesad@shirazu.ac.ir

(Accepted December 14, 2020. First published online: January 13, 2021)

SUMMARY
In this article, a novel mechanism for planar one-legged hopping robots is proposed. The robot consists of a flat foot which is pinned to the leg and a reciprocating mass which is connected to the leg via a prismatic joint. The proposed mechanism performs the hopping by transferring linear momentum between the reciprocating mass and its main body. The nonlinear equations of the motion of the robot are derived using the Euler–Lagrange equations. To accomplish a stable jump, appropriate trajectories have been planned. To guarantee a stable response for this nonlinear system, a sliding-mode controller is implemented. The performance of the hopping robot is investigated through numerical simulations. The results confirm the stability of the hopping robot through the jump cycle on a flat surface and in climbing up and down ramp and stairs.

KEYWORDS: Planar one-legged robot; Trajectory tracking; Hopping; Under-actuated; Sliding mode controller.

1. Introduction

Since the beginning of this millennium, several researchers have studied the hopping robots to pass the obstacles and gaps by jumping over them without getting involved with these barriers. This ability makes the shape of the obstacles or gaps unimportant, and owing to this feature, there is a growing interest in applications. In single-legged robots, the hopping motion is generated in two ways: (1) by pushing the ground according to Newton's third law of motion, a reaction force will be applied to the robot that can be used to accelerate the robot in the upward direction; (2) by making a quick movement toward the ground in some internal part of the robot, according to the conservation of the linear momentum, the rest of the robot picks up an upward velocity.

One of the pioneering studies on the hopping robots was carried out by Raibert[1] for understanding legged systems and proposing a model for hopping robots. The robot consists of a telescopic foot and a body that could make stable jumps and change the direction of jumps by using two actuators. Since then, several researchers have investigated new hopping robot models based on Raibert's model. For instance, Carlesi and Chemori[2] designed a planar hopping robot that imitates the motion of kangaroos during different modes of a jumping gait. You et al.[3] investigated a hopping robot with a mass offset. Zhou et al.[4] designed a hopping robot that is actuated pneumatically and jumps in place. Qian et al.[5] studied a spring-loaded inverse pendulum hopping robot.

Some of the other studies focused on the vertical motion of the hopping robots, and the corresponding mechanisms are similar but with different actuation. The general model contains a leg and a body that is connected to the leg with a prismatic joint and by pushing the ground the robot jumps in place. For instance, Harbrick and Sukhatme[6] proposed the simplest model. This robot was a pogo-stick-like machine and used a pneumatic spring instead of a mechanical spring for storing

* Corresponding author. E-mail: ehsanazadi@shirazu.ac.ir

https://doi.org/10.1017/S0263574720001447 Published online by Cambridge University Press

and releasing the potential energy. Naik and Mehranzadeh[7] investigated the vertical motion of a hopping robot that is pneumatically actuated. Some researchers utilized the crank–slider mechanism to actuate the associated hopping robots.[8,9] Batts et al.[10] designed a hopping robot that uses a voice coil actuator. Hale et al.[11] designed a pneumatically actuated hopping robot.

In recent years, some researchers attempted to develop innovative models. For example, Gunther et al.[12] introduced a new robot named CHIARO that consists of two rigid bodies that are hinged to each other and equipped with a curved foot. Owing to this novel mechanism, the robot was able to make stable jumps without using any sensory feedback. Saar et al.[13] investigated a robot similar to CHIARO which could be equipped with several types of curved feet. Bai et al.[14] designed a symmetric hopping robot named RHop which uses the crank-rocker mechanism to jump. He et al.[15] introduced a hopping robot that consists of an elastic foot and two arms that are hinged to the top of the leg. The robot jumps using the rotational motion of its arms. Zabihi and alasti[16] investigated a one-legged somersaulting robot. In some studies, bio-inspired systems have been used for developing hopping robot models. For example, Wu et al.[17] and Zhu et al.[18] designed human-like one-legged hopping robots. Zhang et al.[19] and Zaitsev et al.[20] investigated locust-inspired hopping robots. Liu et al.[21] and Jun et al.[22] studied kangaroo-inspired hopping robots.

Planning proper trajectories is an important part of locomotion especially for hopping robots. Since the hopping robots are generally an under-actuated system, appropriately designed trajectories are required to guarantee a pre-defined jumping gait for the robot. He et al.[15] planned optimal trajectories to minimize the energy use of the system. Hasaneini et al.[23] introduced an offline method to generate efficient gaits for an articulated one-legged hoping robot. Wu et al.[17] proposed an optimization procedure to maximize the energy efficiency in a hopping gait. Rijnen et al.[24] computed the trajectories of a hopping robot by employing a series of consecutive impact inputs.

Due to the unstable nature of the hopping robots, their control problem is an interesting and complicated subject that has attracted the attention of several researchers. Harbrick and Sukhatme[6] controlled the height of the jumps of a hopping robot using a proportional-derivative (PD) controller by varying the length of the telescopic foot during the stance mode. The dynamic stability of a hopping robot was investigated using a proportional-integral-derivative (PID) controller by Naik and Mehrandezh.[7] A similar analysis was carried out with a neuro-PID controller.[25] A time-varying feedback controller based on the transformation of inputs was presented to stabilize a one-legged hopping robot in ref. [15]. In ref. [2], control of a one-legged hopping robot using a model predictive method was investigated. Zhou et al.[4] proposed a control method which depends on neither external sensors nor estimates of body locations. The proposed method employs a gyroscope to measure the angular velocity of the torso and produce a stable gait consecutively. Azahar et al.[26] integrated a central pattern generator along with proportional-integral (PI) and PID controllers to obtain a stabilizing control input of a one-legged hopper.

Among several one-legged hopping mechanisms that were proposed in the literature, only a handful can travel on rough and irregular terrain. Furthermore, the performance of this distinguished group of hopping mechanisms is extremely limited on irregular terrain. For example, most of the developed mechanisms cannot jump over obstacles that are located too close to the robot such as staircases. Considering the excessive use of service robots in urban pedestrian areas with frequent challenges of ramps and staircases, we aim to develop a one-legged hopping mechanism that can exhibit an acceptable performance in such areas.

In this paper, a novel one-legged hopping robot mechanism with a flat foot is developed. The robot consists of a flat foot and a leg that are hinged together. A tuned-mass mechanism, which consists of an object with a notable mass, is connected to the leg via a prismatic joint. By making a quick movement in tuned-mass toward the ground, the leg picks up an upward velocity and the robot jumps. Meanwhile, the rotation of the leg around the ankle joint enables the robot to move forward through the jumps. The proposed mechanism has two major advantages. First, during the take-off and landing, when only the tip of the foot is in contact with the ground, the dynamics of the robot becomes under-actuated. Due to the under-actuated mode, the robot possesses a special attribute of jumping over extremely close obstacles, while previously proposed mechanisms may fail. Second, the proposed tuned-mass mechanism not only triggers the jump but also stabilizes the landing by lowering the center of mass of the robot as it lands. Planning proper trajectories for hopping gait synthesis has been investigated. To this end, multiple regulation problems have been solved and the resultant trajectories are utilized to design appropriate trajectories to meet the stability and the

https://doi.org/10.1017/S0263574720001447 Published online by Cambridge University Press

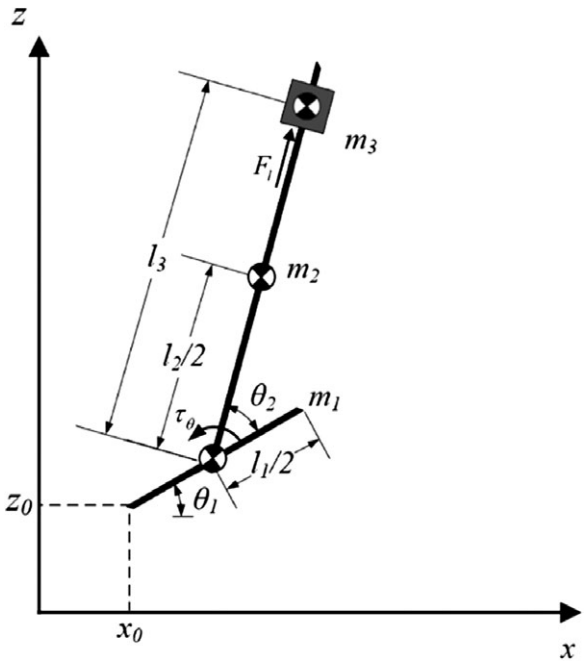


Fig. 1. Schematic model of one-legged hopping robot with a flat foot and a reciprocating mass m_3. The robot has a linear actuator that exerts a force F_l on the mass m_3 and a rotary actuator that applies a torque τ_θ on the leg.

performance requirements. Finally, the sliding mode control method is used to design a stabilizing controller that tracks the designed trajectories with an admissible error. Numerical simulations are employed to investigate the performance of the closed-loop system in various cases of jumping over an obstacle, climbing up/down stairs, and hopping on a ramp. In all cases, a stable hopping gait is successfully achieved by the proposed mechanism in the closed-loop.

2. Hybrid Dynamics of the Hopping Robot

Figure 1 shows the proposed mechanism for the one-legged planar hopping robot. The robot consists of a flat foot and a leg with non-zero masses that are hinged together. A relatively large mass that could make reciprocating motion along the leg is used to pump momentum into the robot for jumping. The flat foot has a length l_1, mass m_1, and inertia J_1. The leg has a length l_2, mass m_2, and inertia J_2, and the object has a notable mass m_3 and inertia J_3. The distance from the ankle to the center of mass (CoM) for the leg is $l_2/2$, and the CoM of the foot is located at its middle point, at the ankle. The generalized coordinates of the model are defined as $(x_0, z_0, \theta_1, \theta_2, l_3)$, where (x_0, z_0) are the coordinates of the heel of the foot, θ_1 is the angle between the foot and the horizontal plane, θ_2 is the angle of the foot relative to the leg, and l_3 is the distance of the tuned-mass from the ankle.

The gait of the robot can be divided into five modes: stance, taking-off under-actuated, flight, landing under-actuated, and recovery (see Fig. 2). In the stance mode, which is the first mode in the jumping gait, the flat foot is rested entirely on the ground. Before the flight mode, the taking-off under-actuated mode happens in which the flat foot starts to rotate around its tip that remains in touch with the ground. At the end of the taking-off under-actuated mode, the flat foot loses its contact with the ground and the robot starts to fly. At the end of the flight mode, the tow of the foot comes in contact with the ground that triggers the landing under-actuated mode. The final mode of the jumping gait is the recovery mode in which the entire length of the flat foot is supported by the ground and the robot is preparing for the next jump by moving toward its initial position. A control torque and a control force are applied to the ankle and prismatic joints, respectively. During all phases of the motion, using these control inputs, desired motions should be achieved. To start a jump, the first step l_3 increases to a desired length. In the second step, a relatively large downward control force is applied to the tuned-mass. Since the control force on the tuned-mass is an internal force, an equal force in the opposite direction applies to the leg at the same time. If the amount of this force

https://doi.org/10.1017/S0263574720001447 Published online by Cambridge University Press

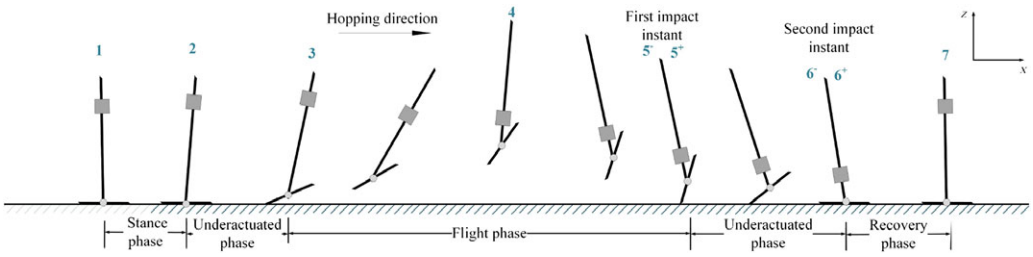


Fig. 2. Stick diagrams of the robot in a hopping cycle.

exceeds a given amount, which will be discussed in detail later, the foot and the leg start to fly. In the following, we will derive the dynamic model of all phases of the gait of the hopping robot including the equations of motion, impacts, and transitions between different modes.

The Euler–Lagrange equations of motion are given by

$$\frac{d}{dt}\left(\frac{\partial T}{\partial \dot{q}_i}\right) - \frac{\partial T}{\partial q_i} + \frac{\partial V}{\partial q_i} = Q^{nc} \tag{1}$$

where T is the kinetic energy, V is the potential energy of the system, q_i is the ith component of the vector generalized coordinates in each mode, and Q^{nc} is the vector of non-conservative generalized forces.

2.1. Stance and recovery modes

In this section, the potential and kinetic energies of the system and other terms of the Euler–Lagrange equations in the stance and recovery modes are derived. Note that the stance and recovery modes essentially have the same dynamic models, but they differ in the control objectives. The heights of the CoM of the leg and the tuned-mass are referred to as z_2 and z_3, respectively, and their horizontal coordinates are denoted by x_2 and x_3, respectively. In the stance and recovery modes, it follows that

$$z_2 = \frac{l_2}{2}\sin(\theta_2) \tag{2}$$

$$z_3 = l_3 \sin(\theta_2) \tag{3}$$

$$x_2 = \frac{l_2}{2}\cos(\theta_2) \tag{4}$$

$$x_3 = l_3 \cos(\theta_2) \tag{5}$$

Therefore, the kinetic energy of the system is given by

$$T_{st} = \frac{1}{2}\left(m_2(\dot{z}_2^2 + \dot{x}_2^2) + m_3\left(\dot{z}_3^2 + \dot{x}_3^2\right) + J_2\dot{\theta}_2^2 + J_3\dot{\theta}_2^2\right) \tag{6}$$

Similarly, the potential energy is given by

$$V_{st} = g\,(m_2 z_2 + m_3 z_3) \tag{7}$$

where g is the gravitational acceleration.

During this phase, $q = [\theta_2\ l_3]^T$ and Q^{nc} is given by

$$Q_{st}^{nc} = \left[\tau_\theta + \tau_f\ \ F_l + F_f\right]^T \tag{8}$$

where τ_θ and F_l are the input torque and force which are applied to the ankle and the object, respectively. The viscous damping torque and force of the ankle and prismatic joint are denoted by τ_f and F_f, respectively, which are given by

$$\tau_f = -c_t\dot{\theta}_2 \tag{9}$$

$$F_f = -c\dot{l}_3 \tag{10}$$

where c_t is the viscous damping coefficient of the revolute joint and c denotes the viscous damping coefficient of the prismatic joint.

https://doi.org/10.1017/S0263574720001447 Published online by Cambridge University Press

2.2. Taking-off and landing under-actuated modes

In the under-actuated modes, the foot starts to rotate around its tip. Therefore, in addition to θ_2 and l_3, θ_1 should also be considered as a generalized coordinate of the system and therefore $q = [\theta_1\ \theta_2\ l_3]^T$. Let the coordinates of the CoM of the foot be (x_1, z_1). It follows that

$$z_1 = \frac{l_1}{2}\sin(\theta_1) \tag{11}$$

$$z_2 = \frac{l_1}{2}\sin(\theta_1) + \frac{l_2}{2}\sin(\theta_1 + \theta_2) \tag{12}$$

$$z_3 = \frac{l_1}{2}\sin(\theta_1) + l_3\sin(\theta_1 + \theta_2) \tag{13}$$

$$x_1 = \frac{l_1}{2}\cos(\theta_1) \tag{14}$$

$$x_2 = \frac{l_1}{2}\cos(\theta_1) + \frac{l_2}{2}\cos(\theta_1 + \theta_2) \tag{15}$$

$$x_3 = \frac{l_1}{2}\cos(\theta_1) + l_3\cos(\theta_1 + \theta_2) \tag{16}$$

The kinetic energy of the system is defined as

$$T_{un} = \frac{1}{2}\left(m_1\left(\dot{z}_1^2 + \dot{x}_1^2\right) + m_2\left(\dot{z}_2^2 + \dot{x}_2^2\right) + m_3\left(\dot{z}_3^2 + \dot{x}_3^2\right) + J_1\dot{\theta}_1^2 + (J_2 + J_3)\left(\dot{\theta}_1 + \dot{\theta}_2\right)^2\right) \tag{17}$$

The potential energy of the system and the Q_{nc} are given by

$$V_{un} = g(m_1 z_1 + m_2 z_2 + m_3 z_3) \tag{18}$$

$$Q_{un}^{nc} = [0\ \tau_\theta + \tau_f\ \ F_l + F_f]^T \tag{19}$$

2.3. Flight mode

In this mode, the robot flies over the ground and the vector of generalized coordinates is $q = [x_0\ z_0\ \theta_1\ \theta_2\ l_3]^T$. It follows that

$$z_1 = z_0 + \frac{l_1}{2}\sin(\theta_1) \tag{20}$$

$$z_2 = z_0 + \frac{l_1}{2}\sin(\theta_1) + \frac{l_2}{2}\sin(\theta_1 + \theta_2) \tag{21}$$

$$z_3 = z_0 + \frac{l_1}{2}\sin(\theta_1) + l_3\sin(\theta_1 + \theta_2) \tag{22}$$

$$x_1 = x_0 + \frac{l_1}{2}\cos(\theta_1) \tag{23}$$

$$x_2 = x_0 + \frac{l_1}{2}\cos(\theta_1) + \frac{l_2}{2}\cos(\theta_1 + \theta_2) \tag{24}$$

$$x_3 = x_0 + \frac{l_1}{2}\cos(\theta_1) + l_3\cos(\theta_1 + \theta_2) \tag{25}$$

Formulation of the potential and kinetic energies of the system in this mode is the same as the under-actuated mode, and the Q_{nc} is given by

$$Q_f^{nc} = \left[0\ 0\ 0\ \tau_\theta + \tau_f\ \ F_l + F_f\right]^T \tag{26}$$

2.4. Impacts

Through the hopping gait, two impacts take place that are assumed to be slip-free. The first impact occurs when the flight mode changes to the under-actuated mode when the heel of the foot touches the ground in the under-actuated mode. The second impact happens when the mode changes from the under-actuated to the recovery. The impacts will be modeled as inelastic impacts, and we will use

https://doi.org/10.1017/S0263574720001447 Published online by Cambridge University Press

the conservation of the angular momentum at the moment of impacts to find the velocity changes. The angular momentum of the system is given by

$$H = \Sigma r_i \times m_i v_i \tag{27}$$

where r_i and v_i denote the position vector to the impact point and the velocity of the CoM for the ith segment of the robot, respectively. The angular velocity of the foot just after the first impact $\dot{\theta}_1^+$ and also the angular velocity of the leg relative to the foot just after the second impact $\dot{\theta}_2^+$ are calculated using the equality of the angular momentum before and after the impact instant. The related derivations are given in Appendix B.

2.5. Transitions between the modes

In this section, the transitions between different modes and the conditions for these transitions are discussed. Through a jumping gait, the first transition occurs between stance and taking-off under-actuated mode. The condition for this transition is that the sum of all torques about the heel becomes negative. The corresponding inequality is given by

$$\begin{aligned} &m_3 g\left(\frac{l_1}{2} + l_3\cos\theta_2\right) + m_2 g\left(\frac{l_1}{2} + \frac{l_2}{2}\cos\theta_2\right) + m_1 g\frac{l_1}{2} + \left(J_2 + J_3 + m_2\frac{l_2^2}{4}\right)\ddot{\theta}_2 \\ &+ m_3\left(2\dot{l}_3\dot{\theta}_2 + l_3\ddot{\theta}_2\right)\left(l_3 + \frac{l_1}{2}\cos\theta_2\right) + m_3\left(\ddot{l}_3 - l_3\dot{\theta}_2^2\right)\frac{l_1}{2}\sin\theta_2 < 0 \end{aligned} \tag{28}$$

If the above condition holds, the robot will begin to rotate about the heel and θ_1 increases; therefore, the under-actuated mode begins. The next transition happens between the taking-off under-actuated and flight modes when the vertical component of the tuned-mass actuator exceeds the sum of the weights of the leg and the foot. This condition is given by

$$(m_1 + m_2)g + F_l\sin(\theta_1 + \theta_2) < 0 \tag{29}$$

The transition from the flight mode to the landing under-actuated mode is the next one. The required condition for this transition is that the robot touches the ground with a non-positive vertical velocity.

During a jumping cycle, the last transition occurs between the landing under-actuated and recovery modes and the necessary condition for this switch can be written as follows:

$$\theta_1 = 0 \;\&\; \dot{\theta}_1 \leq 0 \tag{30}$$

3. Path Planning

Designing appropriate trajectories is an important step to achieve stable jumps. According to Fig. 2, during a jumping cycle, the robot goes through five modes and, during each mode, the trajectories should be designed for specific purposes. Four major purposes that are considered in this research are listed as follows:

- Initiating a jump
- Moving forward during the jump
- Maintaining the stability of the robot
- Preparing for the next jump

The desired trajectories $l_{3d}(t)$ and $\theta_{2d}(t)$ will be designed to achieve the above objectives. Initial conditions for the trajectories (l_{3d}, θ_{2d}) are $(l_{\max}, \pi/2)$. Through the stance mode, l_{3d} is fixed at $l_{\max}$ and θ_{2d} reduces slowly. The forward distance of the jump is strongly affected by the value of θ_2 at the end of the stance mode. As the rotation speed of the leg increases, the robot undergoes a transition to the under-actuated mode. During the under-actuated mode, the objective for designing θ_{2d} is to prepare a condition for the robot to move forward in the flight mode, while l_{3d} is kept fixed at $l_{\max}$. To start a jump, at the last moments of the under-actuated mode, l_{3d} decreases quickly. The quick movement of the mass m_3 lifts the other parts of the robot. Both the stability of the robot during the flight mode and the stability of the gait depend on the movement of the robot through the flight

https://doi.org/10.1017/S0263574720001447 Published online by Cambridge University Press

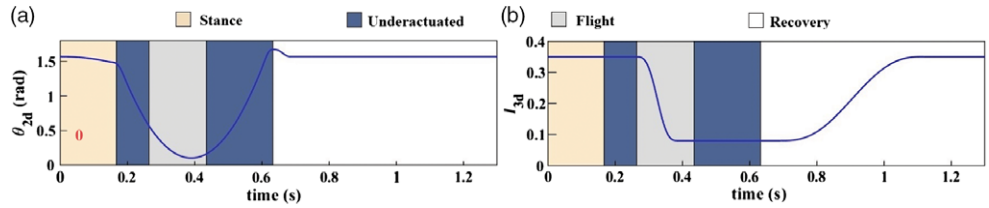


Fig. 3. Designed reference trajectories for a hopping cycle (a) angle of the ankle joint θ_{2d} and (b) displacement of the tuned mass l_{3d}.

mode. During the flight mode, l_{3d} decreases to $l_{\min}$ and remains at this value and θ_{2d} decreases at first and then increases to attain the stability through the upcoming impacts. This increase must be in such a way that the angle between the leg and the horizontal plane $(\theta_1 + \theta_2)$ be greater than $\pi/2$ and maintains at this condition during the under-actuated mode until the second impact instant. Right before the second impact, the velocity of θ_{2d} decreases quickly and this causes a reduction in value of $\dot{\theta}_1$ which improves the stability of the robot through the impact. During the recovery mode, (l_{3d}, θ_{2d}) should return to their initial values and the robot becomes ready for the next jump.

Designed trajectories l_{3d} and θ_{2d} are plotted in Fig. 3, and each mode is separated from the other ones using different colors. According to Fig. 3(a), under-actuated mode starts as the speed of reduction of θ_{2d} becomes large enough; there is a similar relation between reducing l_{3d} and starting the flight mode (see Fig. 3(b)).

4. Sliding Mode Controller Design

To ensure that the robot tracks the desired trajectory of the previous section, a control method should be used that guarantees the stability and performance of the closed-loop system in the presence of disturbances such as air resistance. For the proposed hopping robot, the sliding mode control method is among the most suitable candidates for two reasons. First, it has inherence robustness against disturbances and uncertainties such as air resistance and flexibility of bodies. Second, the sliding mode controller is shown to have a high performance for mechanical systems with similar nonlinear characteristics.[27,28]

To obtain the sliding mode control law, let us express the equations of motion derived in Section 2 as

$$M(q)\ddot{q} + C(q, \dot{q}) = Q^{nc} \tag{31}$$

where M is the inertia matrix and C includes the conservative forces, the Coriolis, and centrifugal terms and gravitational force. As explained in the previous section, the dynamics of the proposed hopping robot is under-actuated. Consequently, the DoFs can be decomposed into a fully actuated and an under-actuated part. The fully actuated dynamics of the hopping robot that is of special importance in the controller synthesis is derived from Eq. (31) as

$$\begin{bmatrix} \cdot & & \\ & \cdot & \\ & & \cdot \\ & m_{\theta\theta} & m_{\theta l} \\ & m_{l\theta} & m_{ll} \end{bmatrix} \begin{bmatrix} \cdot \\ \cdot \\ \cdot \\ \ddot{\theta}_2 \\ \ddot{l}_3 \end{bmatrix} + \begin{bmatrix} \cdot \\ \cdot \\ \cdot \\ c_\theta \\ c_l \end{bmatrix} = \begin{bmatrix} \cdot \\ \cdot \\ \cdot \\ \tau_f + \tau_\theta \\ F_f + F_l \end{bmatrix} \tag{32}$$

Since only trajectories which are aimed to be tracked are trajectories associated with fully actuated dynamics of the system, the under-actuated dynamics of the robot is omitted in the control strategy. Employing the sliding mode control strategy[29] in each mode, two sliding surfaces are defined by

$$s_1 = \left(\frac{d}{dt} + \lambda_1\right) e_\theta \tag{33}$$

$$s_2 = \left(\frac{d}{dt} + \lambda_2\right) e_l \tag{34}$$

https://doi.org/10.1017/S0263574720001447 Published online by Cambridge University Press

Table I. Parameters of the system.

Par.	Value	Unit	Par.	Value	Unit
m_1	0.1	kg	l_1	0.15	m
m_2	0.08	kg	l_2	0.35	m
m_3	0.6	kg	$l_{\max}$	0.35	m
J_1	1.91	kg.cm^2	c_t	1.9	N.m.s.rad^{-1}
J_2	8.17	kg.cm^2	c	0.5	N.s.m^{-1}
J_3	0.9	kg.cm^2	g	9.81	m.s^{-2}

where λ_1 and λ_2 are positive constants, e_θ and e_l are tracking errors defined as $e_\theta = \theta_2 - \theta_{2d}$ and $e_l = l_3 - l_{3d}$.
Taking time derivative of Eqs. (33) and (34) results in

$$\dot{s_1} = -\ddot{\theta}_{2d} + \lambda_1 \dot{e}_\theta + \ddot{\theta}_2 \tag{35}$$

$$\dot{s_2} = -\ddot{l}_{3d} + \lambda_2 \dot{e}_l + \ddot{l}_3 \tag{36}$$

Substituting $\ddot{\theta}_2$ and $\ddot{l}_3$ from Eq. (32) and eliminating the components related to x_0, z_0, and θ_1, Eqs. (35) and (36) can be written in vector form as

$$\begin{bmatrix} \dot{s}_1 \\ \dot{s}_2 \end{bmatrix} = \begin{bmatrix} -\ddot{\theta}_{2d} + \lambda_1 \dot{e}_\theta \\ -\ddot{l}_{3d} + \lambda_2 \dot{e}_l \end{bmatrix} + M_{\theta l}^{-1} \begin{bmatrix} -c_\theta + \tau_f + \tau_\theta \\ c_l + F_f + F_l \end{bmatrix} \tag{37}$$

where

$$M_{\theta l} = \begin{bmatrix} m_{\theta\theta} & m_{\theta l} \\ m_{l\theta} & m_{ll} \end{bmatrix} \tag{38}$$

The control inputs τ_θ and F_l must be chosen such that the following sliding conditions are satisfied

$$\frac{1}{2}\frac{ds_1^2}{dt} \leq -k_1 |s_1| \tag{39}$$

$$\frac{1}{2}\frac{ds_2^2}{dt} \leq -k_1 |s_2| \tag{40}$$

where k_1 and k_2 are positive constants that determines the speed of convergence of the trajectories to s_1 and s_2, respectively. Using Eq. (37) and considering the sliding conditions, the sliding mode control law is obtained as

$$\begin{bmatrix} \tau_\theta \\ F_l \end{bmatrix} = M_{\theta l} \begin{bmatrix} \ddot{\theta}_{2d} - \lambda_1 \dot{e}_\theta - k_1 sgn(s_1) \\ \ddot{l}_{3d} - \lambda_2 \dot{e}_l - k_2 sgn(s_2) \end{bmatrix} + \begin{bmatrix} c_\theta - \tau_f \\ c_l - F_f \end{bmatrix} \tag{41}$$

Generally, the input chattering is a common phenomenon in the sliding mode method which occurs due to discontinuity across the sliding surfaces. To avoid this phenomenon, the saturation functions are utilized instead of sign functions and the modified sliding mode control law is defined as

$$\begin{bmatrix} \tau_\theta \\ F_l \end{bmatrix} = M_{\theta l} \begin{bmatrix} \ddot{\theta}_{2d} - \lambda_1 \dot{e}_\theta - k_1 sat(s_1/\Phi_1) \\ \ddot{l}_{3d} - \lambda_2 \dot{e}_l - k_2 sat(s_2/\Phi_2) \end{bmatrix} + \begin{bmatrix} c_\theta - \tau_f \\ c_l - F_f \end{bmatrix} \tag{42}$$

where Φ_1 and Φ_2 are thin boundary layers around the sliding surfaces s_1 and s_2, respectively.

5. Simulation Results

This section presents the results of the numerical simulations of the closed-loop response of the proposed robot. The parameters of the system are listed in Table I.

https://doi.org/10.1017/S0263574720001447 Published online by Cambridge University Press

Table II. Parameters of controller for each mode.

Mode	Parameters	Values
Stance & Recovery	λ_1	350
	λ_2	19
	k_1	10
	k_2	2
Taking-off under-actuated	λ_1	220
	λ_2	50
	k_1	5
	k_2	1
Flight	λ_1	300
	λ_2	120
	k_1	10
	k_2	0.5
Landing under-actuated	λ_1	350
	λ_2	25
	k_1	1
	k_2	1

The values of the sliding mode controller parameters in each mode are obtained by trial and error and listed in Table II. The values of parameters k_1 and k_2 affect speeds of convergence to the trajectories s_1 and s_2, respectively. Increasing the values of k_1 and k_2 results in a decrease in the closed-loop settling time, but it adversely affects the smoothness of the control inputs (τ_θ and F_l). So, the value of the parameters k_1 and k_2 should be obtained by considering a trade-off between the tracking accuracy and the bandwidth of the control inputs. On the other hand, the values of parameters λ_1 and λ_2 must be chosen as large as possible to decrease the tracking errors (e_θ and e_l). However, large amounts of λ_1 and λ_2 increase the peak value of the control inputs. Considering the above trade-offs, the values of the sliding mode controller parameters in each mode are obtained by trial and error to achieve a fast and accurate closed-loop response with a reasonable control input.

The closed-loop trajectories are plotted in Fig. 4. According to Fig. 4, the desired trajectories have been tracked with a reasonable error and transitions between modes happened at the desired moments. The overall time of the hop cycle is about 1.2 s. However, the flight time is a relatively short portion of the hop cycle duration. The reason is that the proposed robot utilizes a momentum exchange mechanism between the main body of the robot and the tuned-mass. Since the stroke of the tuned-mass actuator is limited, it should accelerate in such a timely manner to produce enough momentum that triggers and supports the flight. Therefore, the duration of the flight phase, which consists of a launch action followed by a free-fall motion, is a small portion of the hop cycle time. The rest of the hop cycle is dedicated to recovery that prepares the robot for the next jump.

As mentioned before, in order to maintain the stability of the robot during the second impact, the angle between the leg and the horizontal plane should be greater than $\pi/2$ (Fig. 4(d)). Moreover, the reduction in the value of $\dot{\theta}_1$, before the second impact, has been aimed and is shown in Fig. 4(c). According to the results, it takes about 1.2 s for the robot to complete one jump.

At the second impact instant, because of the instantaneous change in states of the system, the values of the control inputs may be unreasonable. To avoid this problem, the input torque and input force have been maintained at zero during the second impact instant.

Based on inequality (29), jumping starts when the value of the vertical component of the reaction force that is exerted by the tuned-mass actuator on the main body of the robot (i.e., $F_l \sin(\theta_1 + \theta_2)$) exceeds the sum of the gravitational forces of masses m_1 and m_2 (i.e., $(m_1 + m_2)g$). According to Fig. 5, at the end of taking-off mode and owing to the quick motion of the tuned-mass, inequality (29) is satisfied; consequently, the flight mode begins.

https://doi.org/10.1017/S0263574720001447 Published online by Cambridge University Press

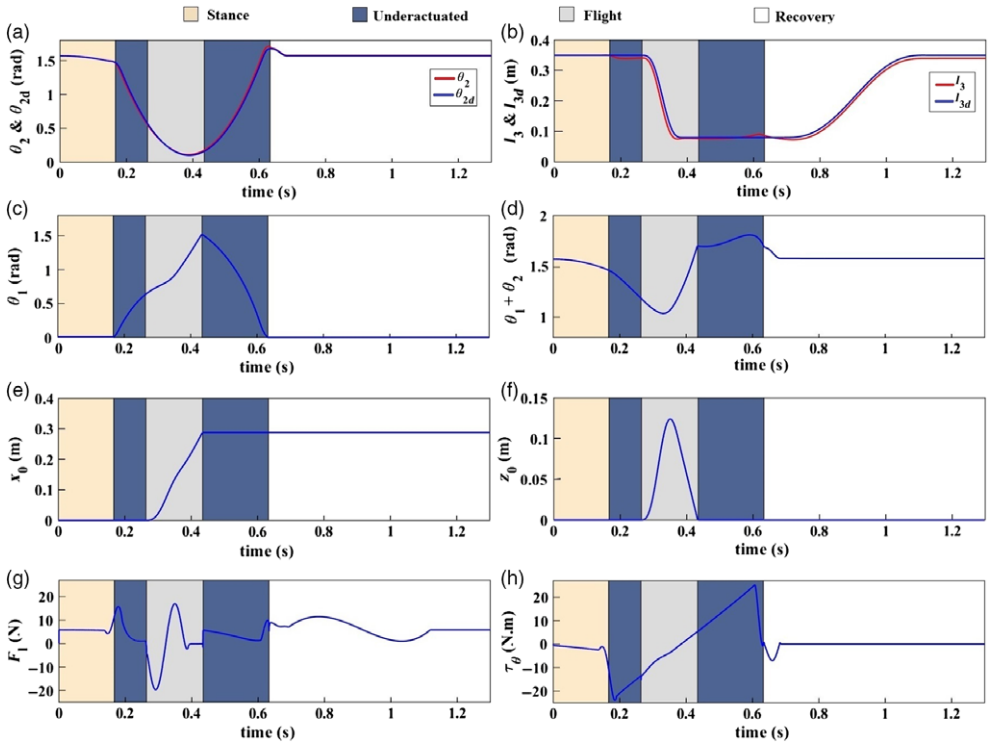


Fig. 4. The closed-loop trajectories of (a) ankle joint rotation θ_2, (b) tuned-mass displacement l_3, (c) flat foot rotation θ_1, (d) the angle between the leg and horizontal plane (θ_1+θ_2), (e) the displacement of heel in horizontal direction x_0, (f) the displacement of heel in vertical direction z_0, (g) the control force F_l, and (h) the control torque τ_θ.

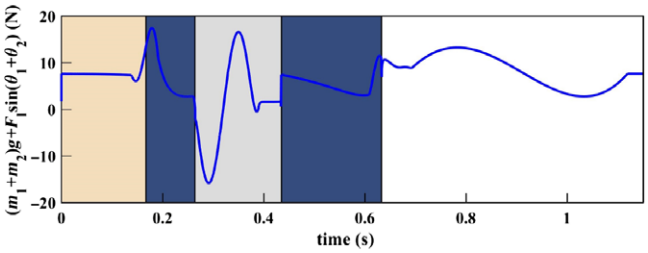


Fig. 5. Second transition condition.

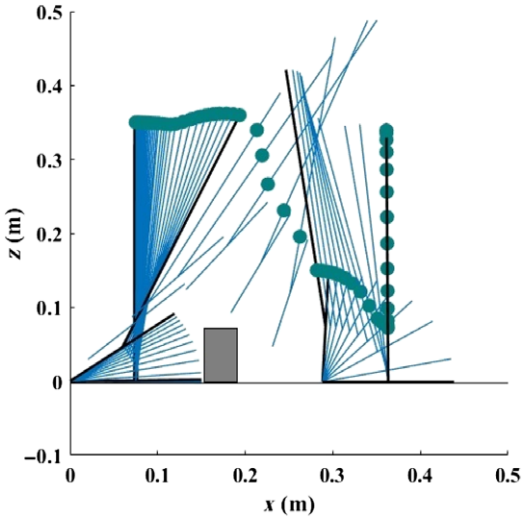


Fig. 6. Stick diagrams of the robot during a hopping cycle.

https://doi.org/10.1017/S0263574720001447 Published online by Cambridge University Press

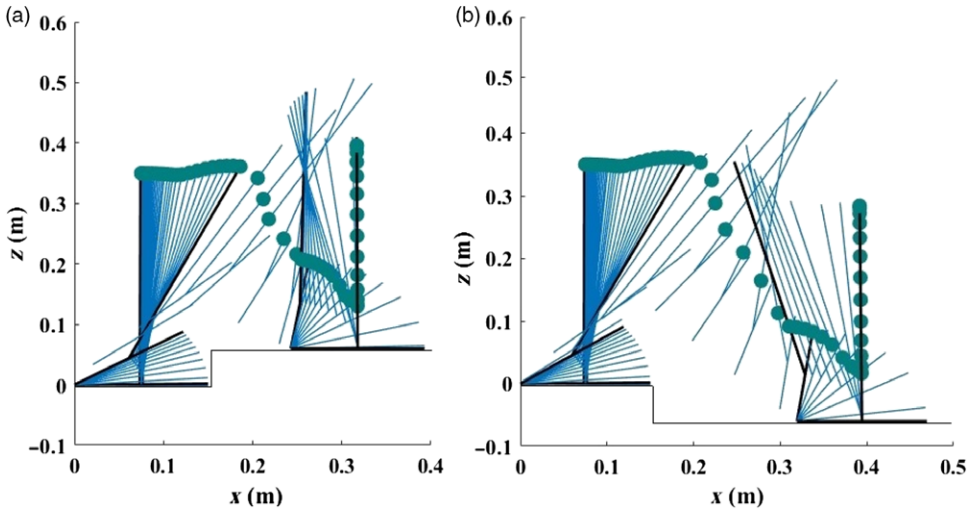


Fig. 7. Stick diagrams of the robot hopping (a) up and (b) down a staircase.

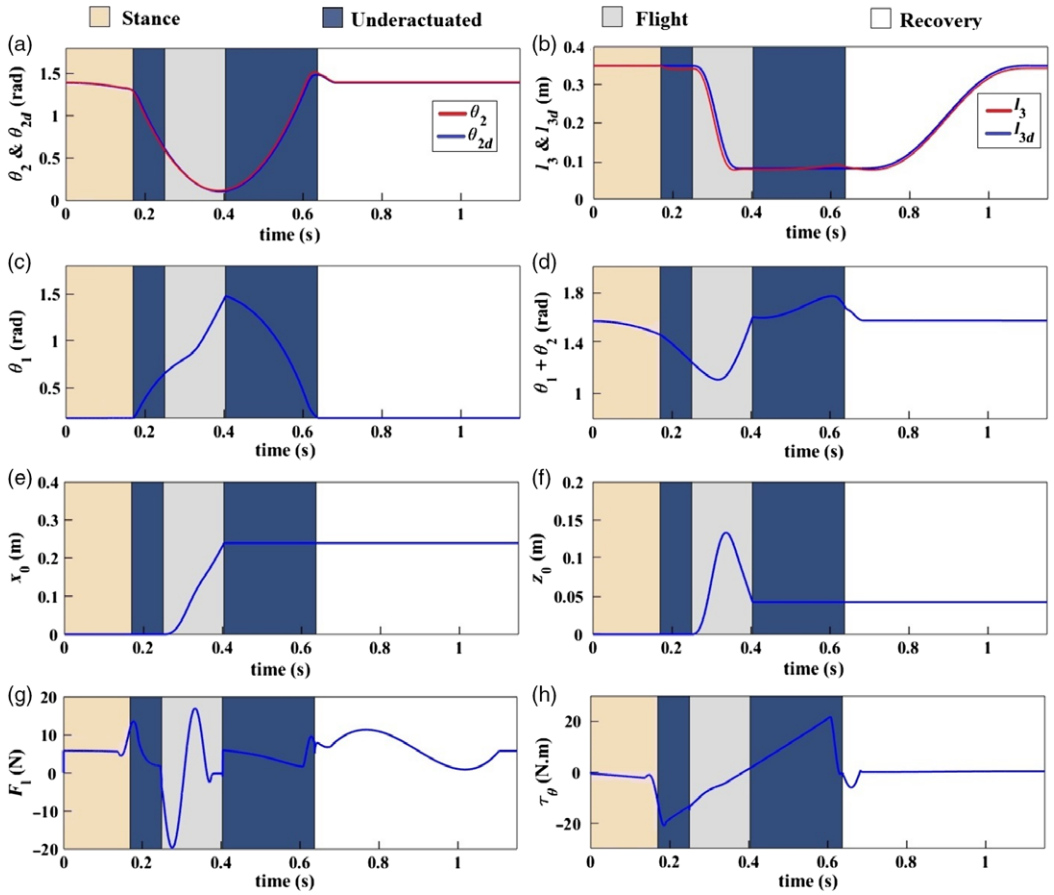


Fig. 8. The closed-loop trajectories for hopping up a staircase with a height of 6 cm, (a) ankle joint rotation θ_2, (b) tuned-mass displacement l_3, (c) flat foot rotation θ_1, (d) the angle between the leg and horizontal plane (θ_1+θ_2), (e) the displacement of heel in horizontal direction x_0, (f) the displacement of heel in vertical direction z_0, (g) the control force F_l, and (h) the control torque τ_θ.

https://doi.org/10.1017/S0263574720001447 Published online by Cambridge University Press

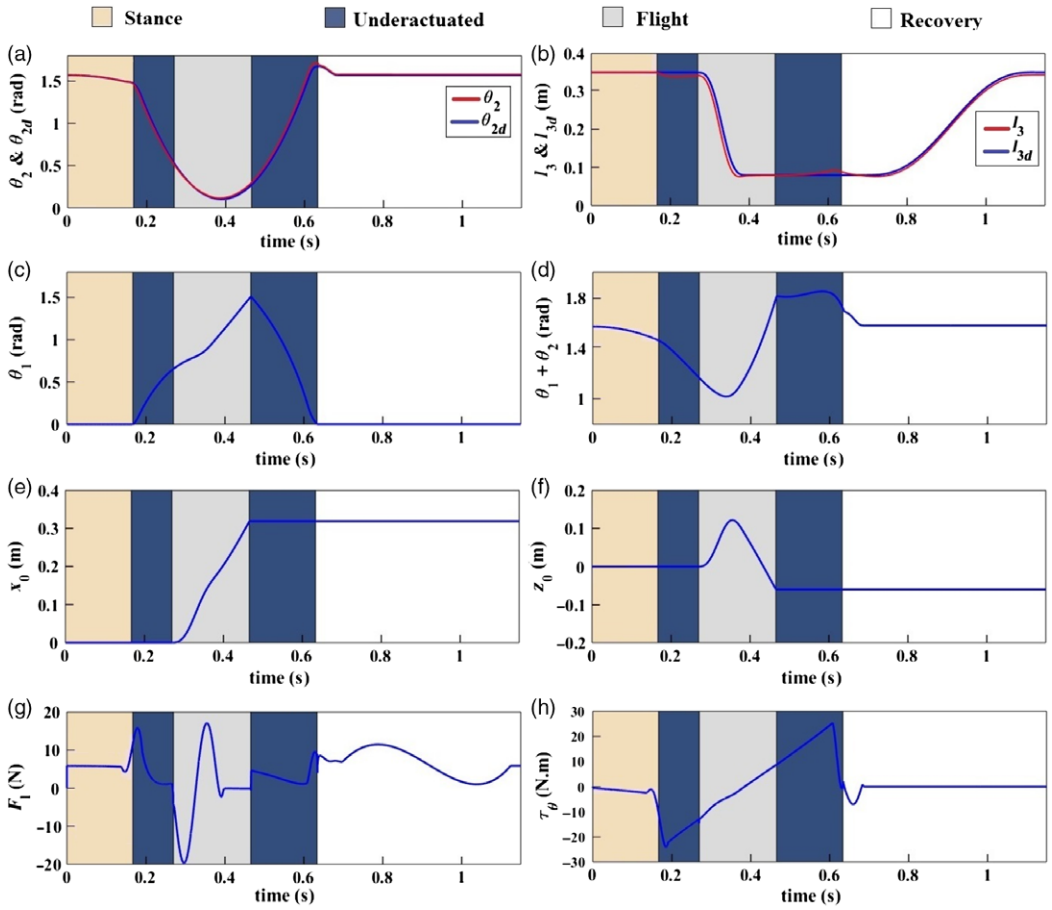


Fig. 9. The closed-loop trajectories for hopping down a staircase with a height of 6 cm, (a) ankle joint rotation θ_2, (b) tuned-mass displacement l_3, (c) flat foot rotation θ_1, (d) the angle between the leg and horizontal plane (θ_1+θ_2), (e) the displacement of heel in horizontal direction x_0, (f) the displacement of heel in vertical direction z_0, (g) the control force F_l, and (h) the control torque τ_θ.

The stick diagrams of the robot in a hopping cycle are shown in Fig. 6. According to the figure, the robot makes a reasonable jump in both vertical and horizontal directions. The robot has a special trait of jumping over the obstacles which is caused by under-actuated mode. According to Fig. 6, through the taking-off under-actuated mode, θ_1 increases that enhances the ability of the robot to jump over close obstacles. In other words, in similar robots, the maximum height of the bottom-most point of the robot occurs approximately in the middle of the jumping distance, but in the current robot, it occurs at the beginning of the gait. Also, the under-actuated mode allows the robot to jump higher by increasing the vertical position of the robot's CoM before the flight mode starts. As shown in Fig. 6, the robot could achieve a hopping distance of 29 cm and a jumping height of 12 cm which means that the robot could jump over gaps with a length of 14 cm and also it could jump over vertical obstacles with a height of 8 cm. Therefore, the flat foot provides the robot with the ability to pass a barrier that is right next to it and conversely other hopping robots could not pass the barriers in this situation and there must be a distance between them and the barriers.

Jumping on irregular surfaces is a challenge for hopping robots. Generally, on an irregular surface, hopping robots with a flat foot are expected to exhibit a relatively more stable response in comparison with the robots with a point contact because the flat foot provides an opportunity for the robot to rest between two consecutive jumps and re-plan the reference trajectory according to the irregularities of the ground. Moreover, the initial and final conditions of a jump cycle can be different in the robots with a flat foot. However, if the irregularities of the surface are unknown, the suitable trajectory cannot be planned easily and it will be the subject of future studies.

Let us study the stability of the proposed mechanism in traveling up and down of a staircase and a slope. The robot has the ability to hop over steps as shown in Fig. 7. According to Fig. 7, the designed

https://doi.org/10.1017/S0263574720001447 Published online by Cambridge University Press

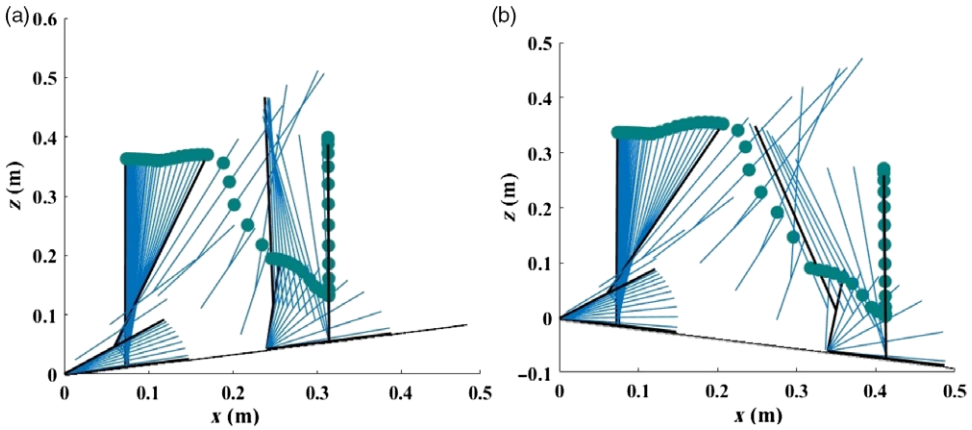


Fig. 10. Stick diagrams of the robot hopping on a ramp (a) with a slope of 10 degrees and (b) a ramp with a slope of −10 degrees.

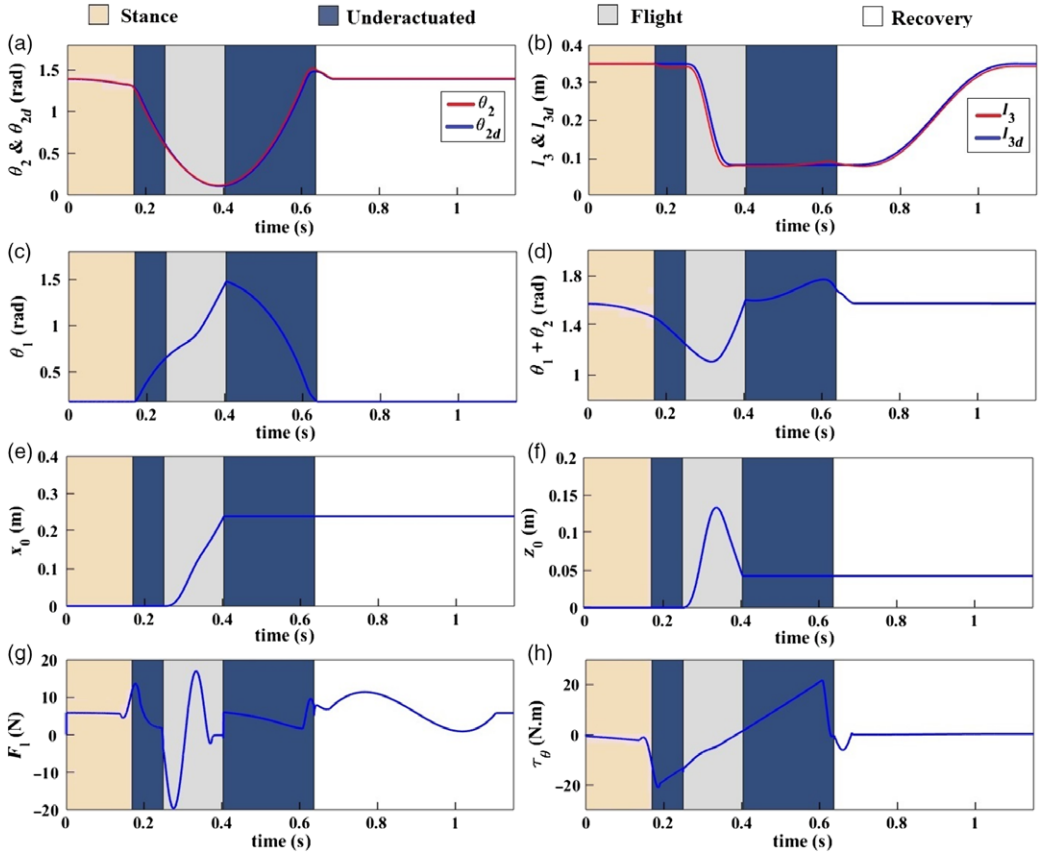


Fig. 11. The closed-loop trajectories for hopping on a ramp with a slope of +10 degrees, (a) ankle joint rotation θ_2, (b) tuned-mass displacement l_3, (c) flat foot rotation θ_1, (d) the angle between the leg and horizontal plane $(\theta_1+\theta_2)$, (e) the displacement of heel in horizontal direction x_0, (f) the displacement of heel in vertical direction z_0, (g) the control force F_l, and (h) the control torque τ_θ.

trajectories of these motions are similar to the regular jump. The robot could jump up a staircase of height 6 cm (Fig. 7(a)). Through jumping up this staircase, the robot has achieved a jumping distance of 27 cm and a maximum height of jump of 11.4 cm. Trajectories have been designed in a way that the robot could jump higher, which has reduced the jumping distance of the robot. Also, the robot could jump down a staircase of height 6 cm which is shown in Fig. 7(b). During this motion, the robot jumps 34 and 8.2 cm in horizontal and vertical directions, respectively, which means the robot jumps longer in comparison to the previous motions (regular jump and jumping up a staircase) but

https://doi.org/10.1017/S0263574720001447 Published online by Cambridge University Press

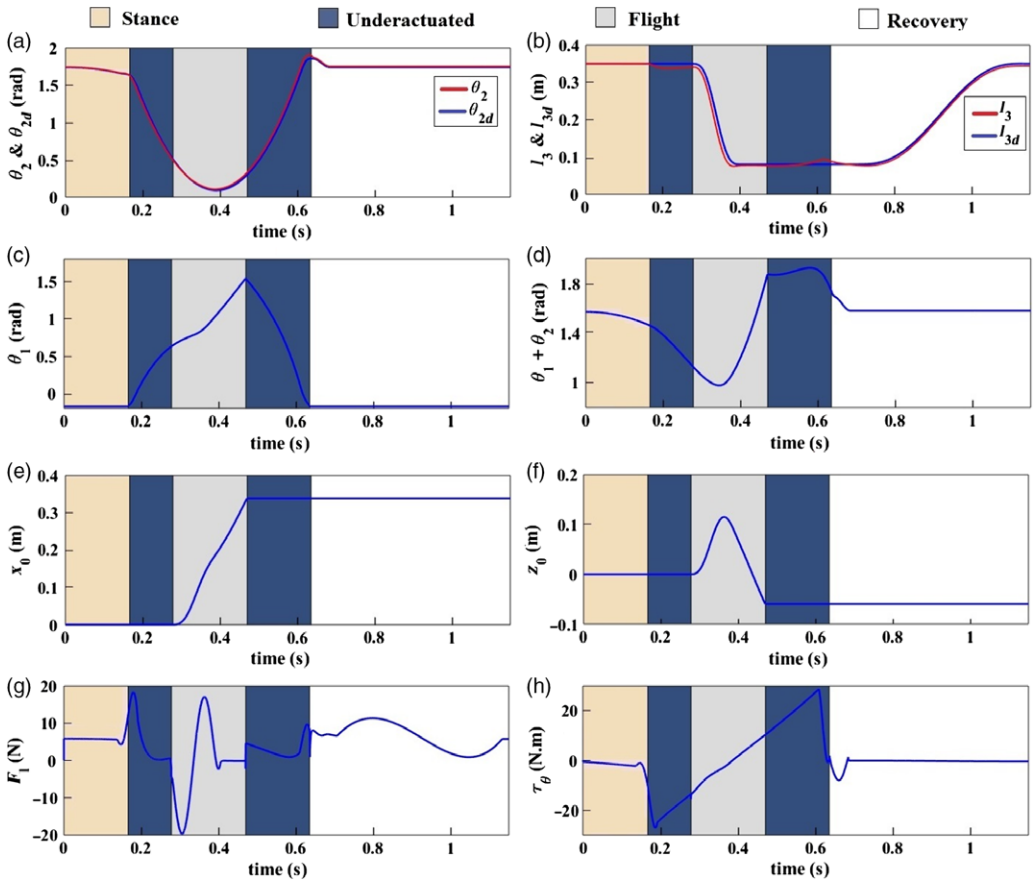


Fig. 12. The closed-loop trajectories for hopping on a ramp with a slope of −10 degrees, (a) ankle joint rotation θ_2, (b) tuned-mass displacement l_3, (c) flat foot rotation θ_1, (d) the angle between the leg and horizontal plane (θ_1+θ_2), (e) the displacement of heel in horizontal direction x_0, (f) the displacement of heel in vertical direction z_0, (g) the control force F_l, and (h) the control torque τ_θ.

the height of the jump has been decreased. The resulting trajectories θ_2 and l_3 and also the resulting trajectories for θ_1, the angle between leg's axis and horizontal plane (θ_1+θ_2), the input torque τ_θ and input force F_l for jumping up and jumping down from the staircase are plotted in Figs. 8 and 9, respectively.

In addition, the closed-loop response of the robot has been investigated on a ramp of +/−10 degrees inclination. The stick diagrams of the mentioned motions are illustrated in Fig. 10. The resulting trajectories θ_2 and l_3 and also the resulting trajectories for θ_1, the angle between leg's axis and horizontal plane (θ_1+θ_2), the input torque τ_θ and input force F_l for jumping on a ramp of +/−10 degrees are plotted in Figs. 11 and 12, respectively. According to Fig. 10, the robot has the ability to make jumps and move forward even on ramped grounds which reveals the adaptability of the robot in different conditions. As shown in Fig. 10(a), a ramp with positive inclinations decreases the average forward velocity of the robot, and according to Fig. 10(b), a slope with negative inclinations enhances the behavior of the robot.

Note that, in practice, the dynamic response of the robot may be affected by phenomena such as frictional impact, air resistance, and elastic impact. Since the above-mentioned phenomena are highly nonlinear, they were not included in our model. However, the inherent robustness of the sliding mode controller may reduce the effect of the un-modeled dynamics on the closed-loop performance.

6. Conclusions

In this paper, a new planar mechanism for hopping robots was proposed. The proposed mechanism consists of a leg, a flat foot, and a reciprocating tuned-mass. To study the dynamics of the robot, the hop cycle was divided into five modes of motion and the nonlinear dynamic model of each mode was derived. The proposed mechanism exhibits two under-actuated modes before and after

https://doi.org/10.1017/S0263574720001447 Published online by Cambridge University Press

the flight mode when the flat foot rotates about its tip that is in contact with the ground. Due to the under-actuated modes, the robot could jump over obstacles that are placed very close to the robot. Appropriate trajectories were designed to achieve four major goals: initiating a jump, moving forward during the jump, the stability of the robot through the flight and landing, and preparing the robot for the next jump. A sliding mode controller was implemented in order to track the designed trajectories. The performance of the proposed robot in closed-loop was investigated through numerical simulations. It was shown that the robot could jump over gaps and obstacles and maintain its stability through the jump cycle. Moreover, a stable hopping gait was achieved in climbing stairs and ramps.

References

1. M. H. Raibert, "Hopping in legged systems–Modeling and simulation for the two-dimensional one-legged case," *IEEE Trans. Syst. Man Cybern.* **14**(3), 451–463 (1984).
2. N. Carlési and A. Chemori, "Nonlinear Model Predictive Running Control of Kangaroo Robot: A One-Leg Planar Under-Actuated Hopping Robot," *2010 IEEE/RSJ International Conference on Intelligent Robots and Systems* (IEEE, 2010) pp. 3634–3639.
3. Y. You, Z. Li, D. G. Caldwell and N. G. Tsagarakis, "From One-Legged Hopping to Bipedal Running and Walking: A Unified Foot Placement Control Based on Regression Analysis," *2015 IEEE/RSJ International Conference on Intelligent Robots and Systems (IROS)* (IEEE, 2015) pp. 4492–4497.
4. Y. Zhou, C. Fu, C. Yun, Z. Yu and K. Chen, "Control of One-Legged Robot Hopping in Place," *2013 IEEE International Conference on Robotics and Biomimetics (ROBIO)* (IEEE, 2013) pp. 1832–1837.
5. H. Qian, L. Sun, R. Qiu and J. Liu, "Varying Velocity Hopping Gait Planning of a One-Legged Robot," *2014 IEEE International Conference on Robotics and Biomimetics (ROBIO 2014)* (IEEE, 2014) pp. 2068–2073.
6. K. Harbick and G. S. Sukhatme, Height control for a onelegged hopping robot using a one-dimensional model, Tech. Rep. IRIS, 01-405 (Institute for Robotics and Intelligent Systems, 2001).
7. K. G. Naik and M. Mehrandezh, "Control of a One-Legged Hopping Robot Using an Inverse Dynamic-Based Pid Controller," *Canadian Conference on Electrical and Computer Engineering, 2005* (IEEE, 2005) pp. 770–773.
8. N. Rahim, A. Kassim, M. Miskon and A. Azahar, "Effectiveness of Central Pattern Generator Model on Developed One Legged Hopping Robot," *2011 IEEE Student Conference on Research and Development* (IEEE, 2011) pp. 85–88.
9. M. Calisti, E. Falotico and C. Laschi, "Hopping on uneven terrains with an underwater one-legged robot," *IEEE Robot. Autom. Lett.* **1**(1), 461–468 (2016).
10. Z. Batts, J. Kim and K. Yamane, Design of a Hopping Mechanism Using a Voice Coil Actuator: Linear Elastic Actuator in Parallel (Leap), *2016 IEEE International Conference on Robotics and Automation (ICRA)* (IEEE, 2016) pp. 655–660.
11. M. F. Hale, J. L. Du Bois and P. Iravani, "Agile and Adaptive Hopping Height Control for a Pneumatic Robot," *2018 IEEE International Conference on Robotics and Automation (ICRA)* (IEEE, 2018) pp. 1–6.
12. F. Günther, F. Giardina and F. Iida, "Self-stable One-Legged Hopping Using a Curved Foot," *2014 IEEE International Conference on Robotics and Automation (ICRA)* (IEEE, 2014) pp. 5133–5138.
13. K. A. Saar, F. Giardina and F. Iida, "Model-free design optimization of a hopping robot and its comparison with a human designer," *IEEE Robot. Autom. Lett.* **3**(2), 1245–1251 (2018).
14. L. Bai, F. Zheng, X. Chen, Y. Sun and J. Hou, "Design and experimental evaluation of a single-actuator continuous hopping robot using the geared symmetric multi-bar mechanism," *Appl. Sci.* **9**(1), 13 (2019).
15. G.-P. He, X.-L. Tan, X.-H. Zhang and Z. Lu, "Modeling, motion planning, and control of one-legged hopping robot actuated by two arms," *Mech. Mach. Theory* **43**(1), 33–49 (2008).
16. M. Zabihi and A. Alasty, "Modeling and Fuzzy Control of One-Legged Somersaulting Robot," *2018 IEEE/RSJ International Conference on Intelligent Robots and Systems (IROS)* (IEEE, 2018) pp. 2701–2706.
17. T.-Y. Wu, T. Yeh and B.-H. Hsu, "Trajectory planning of a one-legged robot performing a stable hop," *Int. J. Robot. Res.* **30**(8), 1072–1091 (2011).
18. Q. Zhu, W. Wu, Y. Zhao, J. Wu and R. Xiong, "Design and Control of Stiffness Coordination Between Knee and Ankle Joints for a Hopping Legged Robot," *2017 IEEE International Conference on Unmanned Systems (ICUS)* (IEEE, 2017) pp. 624–630.
19. Z. Zhang, Q. Yang, S. Gui, B. Chang, J. Zhao, H. Yang and D. Chen, "Mechanism design for locust-inspired robot with one-dof leg based on jumping stability," *Mech. Mach. Theory* **133**, 584–605 (2019).
20. V. Zaitsev, O. Gvirsman, U. B. Hanan, A. Weiss, A. Ayali and G. Kosa, "A locust-inspired miniature jumping robot," *Bioinspiration Biomimetics* **10**(6), 066012 (2015).
21. G.-H. Liu, H.-Y. Lin, H.-Y. Lin, S.-T. Chen and P.-C. Lin, "A bio-inspired hopping kangaroo robot with an active tail," *J. Bionic Eng.* **11**(4), 541–555 (2014).
22. B. Jun, Y. Kim and S. Jung, "Design and Control of Jumping Mechanism for a Kangaroo-Inspired Robot," *2016 6th IEEE International Conference on Biomedical Robotics and Biomechatronics (BioRob)* (IEEE, 2016) pp. 436–440.

https://doi.org/10.1017/S0263574720001447 Published online by Cambridge University Press

23. S. Hasaneini, C. Macnab, J. Bertram and H. Leung, Global Optimum Human-Like Gaits for an Articulated One-Legged Hopper," *2010 IEEE/ASME International Conference on Advanced Intelligent Mechatronics* (IEEE, 2010) pp. 391–396.
24. M. Rijnen, A. van Rijn, H. Dallali, A. Saccon and H. Nijmeijer, "Hybrid trajectory tracking for a hopping robotic leg," *IFAC-PapersOnLine* **49**(14), 107–112 (2016).
25. K. G. Naik, M. Mehrandezh and J. M. Barden, "Control of a One-Legged Hopping Robot Using a Hybrid Neuro-pd Controller," *2006 Canadian Conference on Electrical and Computer Engineering* (IEEE, 2006) pp. 1530–1533.
26. A. H. Azahar, C. S. Horng and A. M. Kassim, "Vertical Motion Control of a One Legged Hopping Robot by Using Central Pattern Generator (CPG)," *2013 IEEE Symposium on Industrial Electronics & Applications* (IEEE, 2013) pp. 7–12.
27. S. Sakaino and K. Ohnishi, "Sliding Mode Control Based on Position Control for Contact Motion Applied to Hopping Robot," *2006 IEEE International Conference on Industrial Technology* (IEEE, 2006) pp. 170–175.
28. H. H. Liou and H. Ming-Tzu, "Hopping Control of a Pneumatic Single-Legged Robot using Sliding Mode Control," *2019 International Automatic Control Conference* (IEEE, 2019) pp. 1–6.
29. J.-J. E. Slotine and W. Li, *Applied Nonlinear Control*, vol. 199 (Prentice hall Englewood Cliffs, NJ, 1991).

Appendix: Explicit Forms of $M(q)$ and $C(q, \dot{q})$ Matrices for Model of Fig. 1 in Stance, Under-Actuated, and Flight Modes

(a) Stance mode

The inertia matrix $M(q)$ for stance mode

$$M = \begin{bmatrix} m_{11} & m_{12} \\ m_{21} & m_{22} \end{bmatrix}$$

in which

$$m_{11} = J_2 + J_3 + m_2 \frac{l_2^2}{4} + m_3 l_3^2 \quad m_{12} = 0 \quad m_{21} = m_{12} \quad m_{22} = m_3$$

The matrix $C(q, \dot{q})$ for stance mode

$$C = [c_{11}\ c_{21}]^T$$

where

$$c_{11} = (m_2 \tfrac{l_2}{2} C_2 + m_3 l_3 C_{12}) g + 2 m_3 l_3 \dot{l}_3 \dot{\theta}_2 \quad c_{21} = -m_3 l_3 \dot{\theta}_2^2 + m_3 g S_2$$

(b) Under-actuated modes

The inertia matrix $M(q)$ for Under-actuated modes

$$M = \begin{bmatrix} m_{11} & m_{12} & m_{13} \\ m_{21} & m_{22} & m_{23} \\ m_{31} & m_{32} & m_{33} \end{bmatrix}$$

in which

$$m_{11} = (m_1 + m_2 + m_3) \tfrac{l_1^2}{4} + \left(m_2 \tfrac{l_2}{2} + m_3 l_3\right) l_1 C_1 + \left(m_2 \tfrac{l_2^2}{4} + m_3 l_3^2\right) + J_! + J_2 + J_3$$

$$m_{12} = \left(m_2 \tfrac{l_2}{2} + m_3 l_3\right) \tfrac{l_1}{2} C_2 + \left(m_2 \tfrac{l_2^2}{2} + m_3 l_3^2\right) + J_1 + J_2 \quad m_{13} = m_3 \tfrac{l_1}{2} S_2 \quad m_{21} = m_{12}$$

$$m_{22} = m_2 \tfrac{l_2^2}{4} + m_3 l_3^2 + J_1 + J_2 \quad m_{23} = 0 \quad m_{31} = m_{13} \quad m_{32} = m_{23} \quad m_{33} = m_3$$

The matrix $C(q, \dot{q})$ for under-actuated modes

$$C = [c_{11}\ c_{21}\ c_{31}]^T$$

https://doi.org/10.1017/S0263574720001447 Published online by Cambridge University Press

in which

$$
\begin{aligned}
c_{11} = &-\left(m_2\frac{l_2}{2}+m_3l_3\right)\frac{l_1}{2}S_2\left(2\dot{\theta}_1+\dot{\theta}_2\right)\dot{\theta}_2+m_3l_1C_2\left(\dot{\theta}_1+\dot{\theta}_2\right)\dot{l}_3+2m_3l_3\dot{l}_3\left(\dot{\theta}_1+\dot{\theta}_2\right)\\
&+m_2\left(\frac{l_1}{2}C_1\dot{\theta}_1+\frac{l_2}{2}C_{12}\left(\dot{\theta}_1+\dot{\theta}_2\right)\right)\left(-\frac{l_1}{2}S_1\dot{\theta}_1-\frac{l_2}{2}S_{12}\left(\dot{\theta}_1+\dot{\theta}_2\right)\right)\\
&+m_2\left(\frac{l_1}{2}S_1\dot{\theta}_1+\frac{l_2}{2}S_{12}\left(\dot{\theta}_1+\dot{\theta}_2\right)\right)\left(\frac{l_1}{2}C_1\dot{\theta}_1+\frac{l_2}{2}C_{12}\left(\dot{\theta}_1+\dot{\theta}_2\right)\right)\\
&-m_3\left(\frac{l_1}{2}C_1\dot{\theta}_1+l_3C_{12}\left(\dot{\theta}_1+\dot{\theta}_2\right)\right)\left(\frac{l_1}{2}S_1\dot{\theta}_1+l_3S_{12}\left(\dot{\theta}_1+\dot{\theta}_2\right)+C_{12}\dot{l}_3\right)\\
&+m_3\left(\frac{l_1}{2}S_1\dot{\theta}_1+l_3S_{12}\left(\dot{\theta}_1+\dot{\theta}_2\right)\right)\left(\frac{l_1}{2}S_1\dot{\theta}_1+l_3S_{12}\left(\dot{\theta}_1+\dot{\theta}_2\right)+S_{12}\dot{l}_3\right)\\
&+\left(m_1\frac{l_1}{2}C_1+m_2\left(\frac{l_1}{2}C_1+\frac{l_2}{2}C_{12}\right)+m_3\left(\frac{l_1}{2}C_1+l_3C_{12}\right)\right)g\\
c_{21} = &-\left(m_2\frac{l_2}{2}+m_3l_3\right)\frac{l_1}{2}S_2\dot{\theta}_1\dot{\theta}_2+m_3\frac{l_1}{2}C_2\left(\dot{\theta}_1+\dot{\theta}_2\right)\dot{l}_3+2m_3l_3\dot{l}_3\left(\dot{\theta}_1+\dot{\theta}_2\right)\\
&+m_2\frac{l_1l_2}{4}S_2\left(\dot{\theta}_1+\dot{\theta}_2\right)\dot{\theta}_1-m_3\left(l_3C_{12}\left(\dot{\theta}_1+\dot{\theta}_2\right)+S_{12}\dot{l}_3\right)\left(-\frac{l_1}{2}S_1\dot{\theta}-l_3s_{12}\left(\dot{\theta}_1+\dot{\theta}_2\right)+C_{12}\dot{l}_3\right)\\
&+m_3\left(-l_3S_{12}\left(\dot{\theta}_1+\dot{\theta}_2\right)+C_{12}\dot{l}_3\right)\left(\frac{l_1}{2}C_1\dot{\theta}+l_3C_{12}\left(\dot{\theta}_1+\dot{\theta}_2\right)+S_{12}\dot{l}_3\right)+\left(m_2\frac{l_2}{2}+m_3l_3\right)C_{12}g\\
c_{31} = &\,m_3\left(\frac{l_1}{2}C_2\dot{\theta}_1^2-l_3\left(\dot{\theta}_1+\dot{\theta}_2\right)^2+S_{12}g\right)
\end{aligned}
$$

(c) Flight mode

The inertia matrix $M(q)$ for flight mode

$$
M=\begin{bmatrix}
m_{11} & m_{12} & m_{13} & m_{14} & m_{15}\\
m_{21} & m_{22} & m_{23} & m_{24} & m_{25}\\
m_{31} & m_{32} & m_{33} & m_{34} & m_{35}\\
m_{41} & m_{42} & m_{43} & m_{44} & m_{45}\\
m_{51} & m_{52} & m_{53} & m_{54} & m_{55}
\end{bmatrix}
$$

where

$$
\begin{aligned}
&m_{11}=m_1+m_2+m_3 \quad m_{12}=0 \quad m_{13}=-\left(m_1+m_2+m_3\right)\tfrac{l_1}{2}S_1-\left(m_2\tfrac{l_2}{2}+m_3l_3\right)S_{12}\\
&m_{14}=-\left(m_2\tfrac{l_2}{2}+m_3l_3\right)S_{12} \quad m_{15}=m_2C_{12} \quad m_{21}=m_{12} \quad m_{22}=m_1+m_2+m_3\\
&m_{23}=\left(m_1+m_2+m_3\right)\tfrac{l_1}{2}C_1+\left(m_2\tfrac{l_2}{2}+m_3l_3\right)C_{12} \quad m_{24}=\left(m_2\tfrac{l_2}{2}+m_3l_3\right)C_{12} \quad m_{25}=m_3S_{12}\\
&m_{31}=m_{13} \quad m_{32}=m_{23}\\
&m_{33}=\left(m_1+m_2+m_3\right)\tfrac{l_1^2}{4}\Big)+\tfrac{3}{2}m_3l_1l_3C_2+\left(m_2\tfrac{l_2^2}{4}+m_3l_3^2\right)+J_1+J_2+J_3\\
&m_{34}=m_2\tfrac{l_1l_2}{4}C_2+m_2\tfrac{l_2^2}{4}+m_3l_3^2+J_1+J_2 \quad m_{35}=m_3\tfrac{l_1}{2}S_2 \quad m_{41}=m_{14} \quad m_{42}=m_{24}\\
&m_{43}=m_{34} \quad m_{44}=m_2\tfrac{l_2^2}{4}+m_3l_3^2+J_1+J_2 \quad m_{45}=0 \quad m_{51}=m_{15} \quad m_{52}=m_{25}\\
&m_{53}=m_{35} \quad m_{54}=m_{45} \quad m_{55}=m_3
\end{aligned}
$$

https://doi.org/10.1017/S0263574720001447 Published online by Cambridge University Press

The matrix $C(q, \dot{q})$ for flight mode

$C = [c_{11}\ c_{21}\ c_{31}\ c_{41}\ c_{51}]^T$

in which

$$c_{11} = -(m_1+m_2+m_3)\frac{l_1}{2}C_1\dot{\theta}_1^2 - \left(m_2\frac{l_2}{2}+m_3l_3\right)C_{12}\left(\dot{\theta}_1+\dot{\theta}_2\right)^2 - 2m_3\dot{l}_3S_{12}\left(\dot{\theta}_1+\dot{\theta}_2\right)$$

$$\begin{aligned}c_{12} = &-(m_1+m_2+m_3)\frac{l_1}{2}S_1\dot{\theta}_1^2 - \left(m_2\frac{l_2}{2}+m_3l_3\right)S_{12}\left(\dot{\theta}_1+\dot{\theta}_2\right)^2 + 2m_3\dot{l}_3C_{12}\left(\dot{\theta}_1+\dot{\theta}_2\right)\\ &+ g(m_1+m_2+m_3)\end{aligned}$$

$$\begin{aligned}c_{31} = &-(m_1+m_2+m_3)\frac{l_1}{2}(\dot{z}_0S_1-\dot{x}_0C_1) + m_3\dot{l}_3(\dot{z}_0S_1-\dot{x}_0C_1)\\ &-\left(m_2\frac{l_2}{2}+m_3l_3\right)(\dot{z}_0C_{12}-\dot{x}_0S_{12})\left(\dot{\theta}_1+\dot{\theta}_2\right) - m_2\frac{l_1l_2}{4}\left(2\dot{\theta}_1+\dot{\theta}_2\right)\dot{\theta}_2 + 2m_3\dot{l}_3l_3\left(\dot{\theta}_1+\dot{\theta}_2\right)\\ &+m_3\frac{l_1}{2}\dot{l}_3C_2\left(3\dot{\theta}_1+4\dot{\theta}_2\right) - m_3\frac{l_1}{2}l_3S_3\left(3\dot{\theta}_1+\dot{\theta}_2\right)\dot{\theta}_2 - m_1\frac{l_1}{2}(\dot{z}_0S_1-\dot{x}_0C_1)\dot{\theta}_1\\ &+m_2\left(\frac{l_1}{2}C_1\dot{\theta}_1+\frac{l_2}{2}C_{12}\left(\dot{\theta}_1+\dot{\theta}_2\right)\right)\left(\dot{x}_0-\frac{l_1}{2}S_1\dot{\theta}_1-\frac{l_2}{2}S_{12}\left(\dot{\theta}_1+\dot{\theta}_2\right)\right)\\ &+m_2\left(\frac{l_1}{2}S_1\dot{\theta}_1-\frac{l_2}{2}S_{12}\left(\dot{\theta}_1+\dot{\theta}_2\right)\right)\left(\dot{z}_0+\frac{l_1}{2}C_1\dot{\theta}_1-\frac{l_2}{2}C_{12}\left(\dot{\theta}_1+\dot{\theta}_2\right)\right)\\ &+m_3\left(\frac{l_1}{2}C_1\dot{\theta}_1+l_3C_{12}\left(\dot{\theta}_1+\dot{\theta}_2\right)-\dot{l}_3S_{12}\right)\left(\dot{x}_0-\frac{l_1}{2}S_1\dot{\theta}_1-l_3S_{12}\left(\dot{\theta}_1+\dot{\theta}_2\right)+\dot{l}_3C_{12}\right)\\ &+m_3\left(\frac{l_1}{2}S_1\dot{\theta}_1+l_3S_{12}\left(\dot{\theta}_1+\dot{\theta}_2\right)-\dot{l}_3C_{12}\right)\left(\dot{z}_0-\frac{l_1}{2}C_1\dot{\theta}_1+l_3C_{12}\left(\dot{\theta}_1+\dot{\theta}_2\right)+\dot{l}_3S_{12}\right)\\ &+\left(m_1\frac{l_1}{2}C_1+m_2\left(\frac{l_1}{2}C_1+\frac{l_2}{2}C_{12}\right)+m_3\left(\frac{l_1}{2}C_1+l_3C_{12}\right)\right)g\end{aligned}$$

$$\begin{aligned}c_{41} = &-\left(m_2\frac{l_2}{2}+m_3l_3\right)(\dot{z}_0S_{12}-\dot{x}_0C_{12})\left(\dot{\theta}_1+\dot{\theta}_2\right) + m_3\dot{l}_3(\dot{z}_0C_{12}-\dot{x}_0S_{12}) + 2m_3l_3\dot{l}_3\left(\dot{\theta}_1+\dot{\theta}_2\right)\\ &-\frac{l_1}{2}\left(m_2\frac{l_2}{2}+m_3l_3\right)S_2\dot{\theta}_1 + m_2\frac{l_2}{2}C_{12}\left(\dot{\theta}_1+\dot{\theta}_2\right)\left(\dot{x}_0-\frac{l_1}{2}S_1\dot{\theta}_1-\frac{l_2}{2}S_{12}\left(\dot{\theta}_1+\dot{\theta}_2\right)\right)\\ &+m_2\frac{l_2}{2}S_{12}\left(\dot{\theta}_1+\dot{\theta}_2\right)\left(\dot{z}_0+\frac{l_1}{2}C_1\dot{\theta}_1+\frac{l_2}{2}C_{12}\left(\dot{\theta}_1+\dot{\theta}_2\right)\right)\\ &+m_3\left(l_3C_{12}\left(\dot{\theta}_1+\dot{\theta}_2\right)-\dot{l}_3S_{12}\right)\left(\dot{x}_0-\frac{l_1}{2}S_1\dot{\theta}_1-l_3S_{12}\left(\dot{\theta}_1+\dot{\theta}_2\right)+\dot{l}_3C_{12}\right)\\ &+m_3\left(l_3S_{12}\left(\dot{\theta}_1+\dot{\theta}_2\right)+\dot{l}_3C_{12}\right)\left(\dot{z}_0+\frac{l_1}{2}C_1\dot{\theta}_1+l_3C_{12}\left(\dot{\theta}_1+\dot{\theta}_2\right)+\dot{l}_3S_{12}\right)+\left(m_2\frac{l_2}{2}+m_3l_3\right)C_{12}g\end{aligned}$$

$$\begin{aligned}c_{51} = &\,m_3(\dot{z}_0C_{12}-\dot{x}_0S_{12})\left(\dot{\theta}_1+\dot{\theta}_2\right) + m_3\frac{l_1}{2}C_1\dot{\theta}_1\dot{\theta}_2\\ &+m_3S_{12}\left(\dot{\theta}_1+\dot{\theta}_2\right)\left(\dot{x}_0-\frac{l_1}{2}S_1\dot{\theta}_1-l_3S_{12}\left(\dot{\theta}_1+\dot{\theta}_2\right)+\dot{l}_3C_{12}\right)\\ &-m_3C_{12}\left(\dot{\theta}_1+\dot{\theta}_2\right)\left(\dot{z}_0+\frac{l_1}{2}C_1\dot{\theta}_1+l_3C_{12}\left(\dot{\theta}_1+\dot{\theta}_2\right)+\dot{l}_3S_{12}\right)+m_3S_{12}g\end{aligned}$$

https://doi.org/10.1017/S0263574720001447 Published online by Cambridge University Press

Impacts
(a) First impact

Angular velocity of the foot after the first impact instant, $\dot{\theta}_1^+$, is given by

$$\begin{aligned}\dot{\theta}_1^+ = &\Bigg[m_1\left(\frac{l_1^2}{4}\dot{\theta}_1^- + (\dot{z}_0 C_1 - \dot{x}_0 S_1)\frac{l_1}{2} + m_2\left(\left(\frac{l_1}{2}C_1 + \frac{l_2}{2}C_{12}\right)\left(\dot{z}_0 + \frac{l_1}{2}\dot{\theta}_1^- C_1 + \frac{l_2}{2}\left(\dot{\theta}_1^- + \dot{\theta}_2\right)C_{12}\right)\right.\right.\\ &\left.-\left(\frac{l_1}{2}S_1 + \frac{l_2}{2}S_{12}\right)\left(\dot{x}_0 - \frac{l_1}{2}\dot{\theta}_1^- S_1 - \frac{l_2}{2}\left(\dot{\theta}_1^- + \dot{\theta}_2\right)S_{12}\right)\right)\\ &+ m_3\left(\left(\frac{l_1}{2}C_1 + l_3 C_{12}\right)\left(\dot{z}_0 + \frac{l_1}{2}\dot{\theta}_1^- C_1 + l_3\left(\dot{\theta}_1^- + \dot{\theta}_2\right)\right.\right.\\ &\left.-\left(\frac{l_1}{2}S_1 + l_3 S_{12}\right)\left(\dot{x}_0 - \frac{l_1}{2}\dot{\theta}_1^- S_1 - l_3\left(\dot{\theta}_1^- + \dot{\theta}_2\right)S_{12} + \dot{l}_3 C_{12}\right) + J_1\dot{\theta}_1^- + (J_2 + J_3)\left(\dot{\theta}_1^- + \dot{\theta}_2\right)\right.\\ &-m_2\left(\frac{l_2^2}{4} + \frac{l_1 l_2}{4}C_2\right)\dot{\theta}_2 + m_3\left(\frac{l_3^2}{4} + \frac{l_1 l_3}{2}C_2\right)\dot{\theta}_2 + m_3\frac{l_1}{2}S_2\dot{l}_3 + (J_2 + J_3)\Bigg]\Bigg/\Bigg[(m_1 + m_2 + m_3)\frac{l_1^2}{4}\\ &+ m_2\frac{l_1^2}{4} + m_3 l_3^2 + m_2\frac{l_1}{2}l_2 C_2 + m_3 l_1 l_3 C_2 + J_1 + J_2 + J_3\Bigg]\end{aligned}$$

where $\dot{\theta}_1^-$ is the instant angular velocity of the foot before the impact instant.

(b) Second impact

Angular velocity of the leg relative to the foot after the second impact instant, $\dot{\theta}_2^+$, is given by

$$\begin{aligned}\dot{\theta}_2^+ = &\left((m_1 + m_2 + m_3)\frac{l_1^2}{4}\dot{\theta}_1 + m_2\left(\frac{l_2^2}{4}\left(\dot{\theta}_1 + \dot{\theta}_2^- + \frac{l_1 l_2}{2}C_2\left(\dot{\theta}_1 + \dot{\theta}_2^-\right)\right) + J_1\dot{\theta}_1\right) + (J_1 + J_2)\left(\dot{\theta}_1 + \dot{\theta}_2^-\right)\right.\\ &\left.+m_3\left(l_3^2\left(\dot{\theta}_1 + \dot{\theta}_2^-\right) + \frac{l_1}{2}l_3 C_2\left(\dot{\theta}_1 + \dot{\theta}_2^-\right) + \frac{l_1}{2}\dot{l}_3 S_2\right)\right) \Big/ \left(m_2\frac{l_2^2}{4} + m_3 l_3^2 + J_2 + J_3\right)\end{aligned}$$

where $\dot{\theta}_2^-$ is the instant angular velocity of the foot before the impact instant.

https://doi.org/10.1017/S0263574720001447 Published online by Cambridge University Press